Journal of Thermal Analysis and Calorimetry, Vol. 94 (2008) 3, 719–726

THERMAL DEGRADATION AND COMBUSTION BEHAVIOR OF THE POLYETHYLENE/CLAY NANOCOMPOSITE PREPARED BY MELT INTERCALATION

S. M. Lomakin[1*], *I. L. Dubnikova*[2], *A. N. Shchegolikhin*[1], *G. E. Zaikov*[1], *R. Kozlowski*[3], *G.-M. Kim*[4] *and G. H. Michler*[4]

[1]NM Emanuel Institute of Biochemical Physics of Russian Academy of Sciences, 119934 Kosygin 4, Moscow, Russia
[2]NN Semenov Institute of Chemical Physics of Russian Academy of Sciences 119991 Kosygin 4, Moscow, Russia
[3]Institute of Natural Fibres, ul. Wojska Polskiego 71 b, Poznan, Poland
[4]Martin-Luther-Universität Halle-Wittenberg, Geusaer Straße, 06217 Merseburg, Germany

Studies of thermal and fire-resistant properties of the polyethylene/organically modified montmorillonite (PE/MMT) nanocomposites prepared by means of melt intercalation are discussed. The sets of the data acquired with the aid of non-isothermal TG experiments have been treated by the model kinetic analysis. The extra acceleration of thermal-oxidative degradation of the nanocomposite which has been observed at the first stage of the overall process has been analyzed and is explained by the catalytic effect of the clay nanoparticles. The results of cone calorimetric tests lead to the conclusion that char formation plays a key role in the mechanism of flame retardation for nanocomposites.

Keywords: *combustion, intercalation polymerization, kinetics, layered clay, nanocomposite, oxidation, polyethylene, thermal degradation*

Introduction

The properties and thermal degradation of model polyethylene (PE) are reasonably well known [1–12]. It is generally accepted that pristine PE has relatively low thermal stability and flame resistance. The approach to the enhancement of thermal stability and fire resistance based on the use of polymer nanocomposites has been extensively developed in the last years [13–19].

Intercalation in polymer melts is widely used as a simple method for the synthesis of corresponding materials [18]. In these experimental studies, it was found that PE nanocomposites based on layered silicates exhibit lower flammability as compared with the parent polymer, which can be achieved by introducing a small amount of an inorganic silicate ingredient [13–16].

It is believed that, in the course of high temperature pyrolysis and/or combustion, clay nanoparticles are capable of promoting formation of protective clay-reinforced carbonaceous char which is responsible for the reduced mass loss rates, and hence the lower flammability.

Alongside with an enhancement of flame resistance of such nanocomposites the rise of thermal stability observed during TG experiments. Generally, TG cannot be used to elucidate a complex mechanism of polymer thermal degradation. Nevertheless, dynamic TG has been frequently used to study the overall thermal degradation kinetics of polymers because it gives reliable information on the kinetic parameters, such as preexponential factor, the activation energy, and the overall reaction order [20–22]. The thermal degradation kinetics of polyethylene has been studied by many investigators. Various suggestions for the kinetic parameters for polymer degradation have been reported [8–10, 20–22]. Although some attempts have been made to understand the complex nature of decomposition of a polymer, involving numerous reactions, some authors have found it sufficient to consider a global first order kinetic expression to represent the overall decomposition rate [8].

In this work we applied the model kinetic analysis of PE and PE/MMT thermal-oxidative degradation in order to predict an increase of flame resistance for PE nanocomposite, i.e. the reduction of the mass loss rate and the rate of heat release.

Experimental

Materials

PE, Basel Lupolen, was used to prepare PE nanocomposites in the combinations with polar compatibilizer,

* Author for correspondence: lomakin@sky.chph.ras.ru

1388–6150/$20.00
© 2008 Akadémiai Kiadó, Budapest
Akadémiai Kiadó, Budapest, Hungary
Springer, Dordrecht, The Netherlands

maleic anhydride-modified oligomer (MAPE) Polybond 3109, provided by Crompton. A Cloisite 20A (purchased from Southern Clay Products, Inc.) has been used as the organically modified montmorillonite (MMT) to prepare PE-MMT and PE-MAPE-MMT nanocomposites throughout this study. The content of an organic cation-exchange modifier, N^+2CH_32HT (HT=hydrogenated tallow, C18≈65%; C16≈30%; C14≈5%; anion: Cl^-), in the MMT was of 38 mass%.

Preparation of nanocomposites

PE/MAPE/MMT nanocomposites were prepared by the melt mixing of the components in a double-rotor laboratory (Brabender) mixer in two steps. PE and maleic anhydride-modified oligomer (MAPE – Polybond 3109 by Crompton Co.) were blended/mixed using a laboratory Brabender mixing chamber in two steps. In the first step, the two polymers PE and MAPE were blended in a 4:1 ratio for 2 min; after that, an MMT powder was added in an amount of 3 and 7 mass%. The mixing of components at the second step lasted for 10 min at a temperature of 190°C and rotor speeds of 60 rpm. Samples designed for cone calorimeter testing in the form of 70×70×3 mm plates with a mass of 14.0±0.1 g were prepared by molding at 190°.

Investigation techniques

Transmission electron microscopy (TEM)

The filler dispersion in the composites was studied by the TEM technique with a Philips EM-301 electron microscope (the Netherlands) at an accelerating voltage of 80 kV. Thin sections of film samples for TEM examination were prepared with an LKB Ultratome III® ultramicrotome.

Thermogravimetric analysis (TG)

A Perkin-Elmer TGA-7 instrument calibrated by Curie points of several metal standards has been employed for non-isothermal thermogravimetric analysis. The measurements were carried out at a desired heating rate (in the range of 2.5–10 K min^{-1}) in air. A kinetic analysis of the thermal degradation of composites was performed with the use of the Netzsch-Gerätebau Thermokinetics software. The algorithm of the kinetic analysis program was based on the calculation of regression by the fifth-order Runge–Kutta method using the dedicated Prince–Dormand formula for automatic optimization of the number of significant digits [23, 24].

Combustibility characteristics (cone calorimeter)

Ignitability tests were performed according to the standard procedures ASTM 1354-92 and ISO/DIS 13927 using a cone calorimeter [25].

Results and discussion

Investigation of nanocomposite structure

TEM technique has been used to evaluate the degree of exfoliation of the organoclay particles in the polymer matrix. Figures 1–3 show the influence of polar compatibilizer (MAPE) on the exfoliation degree of the MMT in the nanocomposites.

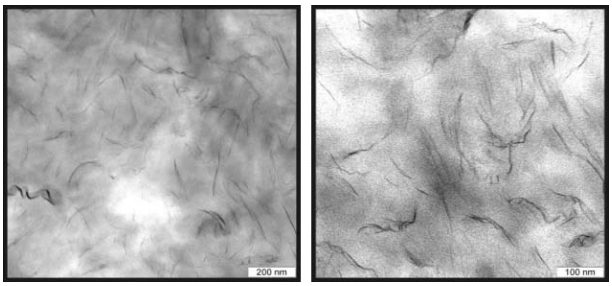

Fig. 1 TEM micrographs of MAPE-7 mass% Cloisite 20A – maleic anhydride-modified PE oligomer (Polybond 3109) at different magnification showing mainly exfoliated nanocomposite

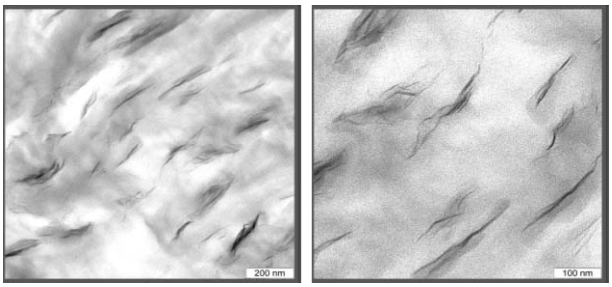

Fig. 2 TEM micrographs of PE-MAPE-7 mass% Cloisite 20A at different magnification showing discrete (hybrid) structure of nanocomposite consisting of intercalated tactoids and exfoliated monolayers

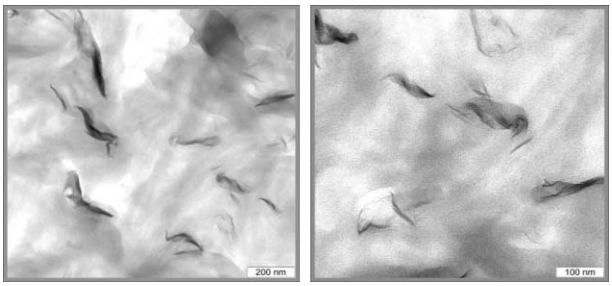

Fig. 3 TEM micrographs of PE-7 mass% Cloisite 20A at different magnifications (for the most part intercalated nanocomposite)

It is seen that the full exfoliation of the MMT particles to the monolayers takes place under the action of maleic anhydride-modified PE compatibilizer in the MAPE-MMT nanocomposite (Fig. 1), whereas in the PE-MAPE-MMT nanocomposite the hybrid structure of consisting of intercalated tactoids and exfoliated MMT monolayers has been formed (Fig. 2). Finally, the pure PE-MMT composition has the intercalated structure of nanocomposite (Fig. 3).

Study of thermal-oxidative degradation of PE-MAPE-MMT nanocomposite

It is acknowledged that thermal stability of polymer nanocomposites is higher than that of pristine polymers, and this gain is explained by the presence of anisotropic clay layers hindering diffusion of volatile products through the nanocomposite material.

The radical mechanism of thermal degradation of PE has been widely discussed in a framework of random scission type reactions [1–10]. It is known that PE decomposition products comprise a wide range of alkanes, alkenes and dienes. The polymer matrix transformations, usually observed at lower temperatures and involving molecular mass alteration without formation of volatile products, are principally due to the scission of weak links, e.g. oxygen bridges, incorporated into the main chain as impurities. The kinetics of thermal degradation of PE is frequently described by a first-order model of mass conversion of the sample [10, 21]. A broad variation in Arrhenius parameters can be found in literature, i.e., activation energy (E) ranging from 160 to 320 kJ mol^{-1} and pre-exponential factor (A) variations in the range of 10^{11} and 10^{21} s^{-1} [7–10] are not unusual. It is believed that the broad range of E values reported may be explained by the polymers molecular mass variations, by use of various additives, and by different experimental conditions [10] employed by different authors.

Thermal-oxidative degradation of PE and PE nanocomposites has been extensively studied over the past decades [26–28, 14–17]. It has been reported that the main oxidation products of PE are aldehydes, ketons, carboxylic acids, esters and lactones [26, 27]. According to [26], β-scission plays an important role in thermal oxidation of UHMWPE. Notably, the feasibility of intra-molecular hydrogen abstraction by the peroxy radicals for polyethylene has been questioned in frames of a thermal oxidation mechanism proposed by Gugumus [27, 28]. A mechanism describing oxidation of organic molecules by virtue of complex chain reactions has been proposed earlier by Benson [29].

In the present work, the processes of thermal degradation of PE and PE-MAPE-MMT nanocomposite with MMT content of 7 mass% have been investigated by TG in an air at the heating rates of 2.5, 5 and 10 K min^{-1}. According to the dynamic TG data, the polymer thermal-oxidative degradation starts at about 300°C and then, through a complex radical chain process, the material totally destructs and completely volatilizes in the range of 450–500°C (Fig. 4).

The diverse behavior of PE and PE-MAPE-MMT (Figs 4 and 5) shows that the influence of MMT nanoparticles on the thermal-oxidation process resulted in higher thermal-oxidative stability of hybrid PE-MAPE-MMT nanocomposite. It can be seen a regular increase in the temperature values of the maximum mass loss rates (about 50°C) for the PE-MAPE-MMT as compared to pristine PE (Fig. 5).

It seems reasonable to suggest that thermally stable crosslinked carbonized layer on the nanocomposite surface is formed during the thermal-oxidative degradation and starts to hinder the diffusion transport of both the volatile degradation products (out of the polymer melt into the gas phase) and the oxygen (from the gas phase into the polymer). The above set of events results in actual increase of the nanocomposite thermal stability in the temperature range of 350–500°C, where normally a general degradation of the main part of PE takes place.

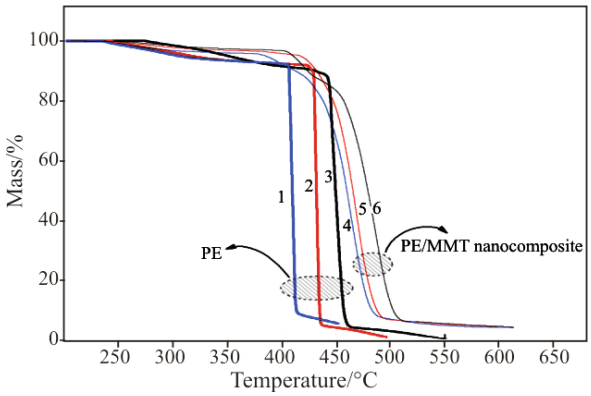

Fig. 4 TG curves for PE (1 – 2.5, 2 – 5, 3 – 10 K min^{-1}) and PE-MAPE-MMT (4 – 2.5, 5 – 5, 6 – 10 K min^{-1})

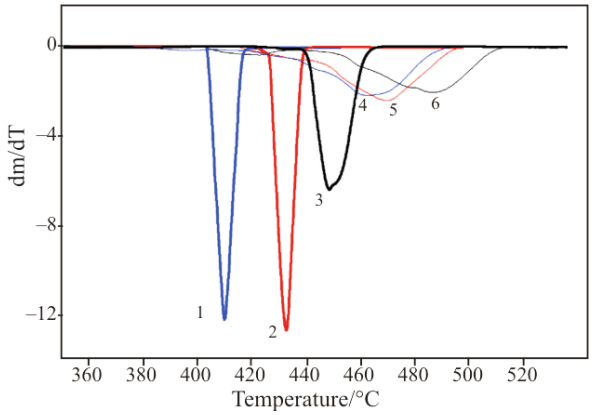

Fig. 5 DTG curves for PE (1 – 2.5, 2 – 5, 3 – 10 K min^{-1}) and PE-MAPE-MMT (4 – 2.5, 5 – 5, 6 – 10 K min^{-1})

Kinetic analysis of PE-MAPE-MMT thermal oxidative degradation

Kinetic studies of material degradation have long history, and there exists a long list of data analysis techniques employed for the purpose. Often, TG is the method of choice for acquiring experimental data for subsequent kinetic calculations, and namely this technique was employed here.

It is commonly accepted that the degradation of materials follows the base Eq. (1) [23]

$$dc/dt = -F(t,Tc_0c_f) \quad (1)$$

where t – time, T – temperature, c_0 – initial concentration of the reactant, and c_f – concentration of the final product. The right-hand part of the equation $F(t,T,c_0,c_f)$ can be represented by the two separable functions, $k(T)$ and $f(c_0,c_f)$:

$$F(t,T,c_0,c_f)=k[T(t)f(c_0,c_f)] \quad (2)$$

Arrhenius Eq. (4) will be assumed to be valid for the following:

$$k(T)=A\exp(-E/RT) \quad (3)$$

Therefore,

$$dc/dt = -A\exp(-E/RT)f(c_0,c_f) \quad (4)$$

All feasible reactions can be subdivided onto classic homogeneous reactions and typical solid-state reactions, which are listed in Table 1 [23]. The analytical output must provide good fit to measurements with different temperature profiles by means of a common kinetic model.

Kinetic analysis of thermal oxidative degradation of PE and PE-MAPE-MMT at the heating rates of 2.5, 5 and 10 K min^{-1} (Figs 6a and b) has been accomplished by using the interactive model based nonlinear fitting approach in accordance with a formalism we proposed earlier [30]. In order to assess the activation energy for development of a reasonable model for kinetic analysis of pristine PE and PE-MAPE-MMT thermal degradation processes, a few evaluations by model-free Friedman analysis have been done as the starting point [31].

Further, nonlinear model fitting procedure for PE and PE-*n*-MMT TG-curves has led to the following triple-stage model scheme of successive reactions, wherein a general n^{th}-order (F_n) reaction was used for all steps of the overall process of thermal oxidative degradation (Table 1) (Figs 6a and b):

$$A \xrightarrow{F_n} B \xrightarrow{F_n} C \xrightarrow{F_n} D \quad (5)$$

Table 1 Reaction types and corresponding reaction equations, $dc/dt = -A\exp(-E/RT)f(c_0,c_f)$

Name	$f(c_0,c_f)$	Reaction type
F_1	c	first-order reaction
F_2	c^2	second-order reaction
F_n	c^n	n^{th}-order reaction
R_2	$2c^{1/2}$	two-dimensional phase boundary reaction
R_3	$3c^{2/3}$	three-dimensional phase boundary reaction
D_1	$0.5/(1-c)$	one-dimensional diffusion
D_2	$-1/\ln c$	two-dimensional diffusion
D_3	$1.5e^{1/3}(c^{-1/3}-1)$	three-dimensional diffusion (Jander's type)
D_4	$1.5/(c^{-1/3}-1)$	three-dimensional diffusion (Ginstling–Brounstein type)
B_1	c_0c_f	simple Prout–Tompkins equation
B_{na}	$c_0^n c_f^a$	expanded Prout–Tompkins equation (n_a)
C_{1-X}	$c(1+K_{cat}X)$	first-order reaction with autocatalysis through the reactants, X. $X=c_f$
C_{n-X}	$c^n(1+K_{cat}X)$	n^{th}-order reaction with autocatalysis through the reactants, X
A_2	$2c(-\ln c)^{1/2}$	two-dimensional nucleation
A_3	$3c(-\ln c)^{2/3}$	three-dimensional nucleation
A_n	$Nc(-\ln c)^{(n-1)/n}$	n-dimensional nucleation/nucleus growth according to Avrami/Erofeev

As data in Table 2 for the first stage of thermal oxidative degradation reaction show, the activation energies values for PE and PE-MAPE-MMT amount to 65.5 and 87.5 kJ mol^{-1}, thus indicating that the degradation of these samples is initiated by the similar oxygen induced reactions.

At the second stage, the lower activation energy of PE-*n*-MMT (166.2 kJ mol^{-1}) compared to that of PE (238 kJ mol^{-1}) may be related to the catalytic influence of MMT on the thermal oxidation of PE. At the same time, the values of activation energy found at the third stage of thermal-oxidative degradation for PE-*n*-MMT (279.6 kJ mol^{-1}) are higher than those for PE (250.2 kJ mol^{-1}) (Table 2). This difference may be attributed to a shift of the PE-*n*-MMT degradation process to a diffusion-limited mode owing to emergence in the system of a carbonized cross-linked material. It is known [11] that the contribution of radical recombination reactions, which lead to the intermolecular crosslinking, increases under the oxygen deficiency conditions. Such conditions are realized at thermal oxidative degradation of the PE nanocomposites due to the labyrinth effect of the silicate layers towards the diffusing gas. The formation of chemical crosslinking during the thermal-oxidative degradation of the PE nanocomposites is a necessary condition of PE carbonization process.

This fact infers that the last stage of the PE-*n*-MMT degradation process is governed mainly by random scission of C–C bonds, rather than by an oxygen catalyzed reactions. On the other hand, these results are also consistent with the barrier model mechanism, which suggests that inorganic clay layers can play a role of barriers retarding the diffusion of oxygen from gas phase into the nanocomposite.

On the basis of the calculated kinetic parameters of thermal-oxidative degradation of PE and PE-MAPE-MMT, we designed the curves of mass loss rate during the isothermal (600°C) heating of the samples over 60 s (Fig. 7). The choice of the specified temperature 600°C is not occasional, since this temperature corresponds to an incident heat flux of 35 kW m^{-2} that has been used in working tests on the ignitability of samples with a cone calorimeter [25]. The tests made it possible to evaluate important combustibility characteristics, such as mass loss rate and heat release rate. The calculation of the heat release rate as a fundamental parameter measured by the cone calorimeter was based on the oxygen absorption principle. According to this principle, the heat released during the burning of a material is proportional to the amount of oxygen required for its combustion. For

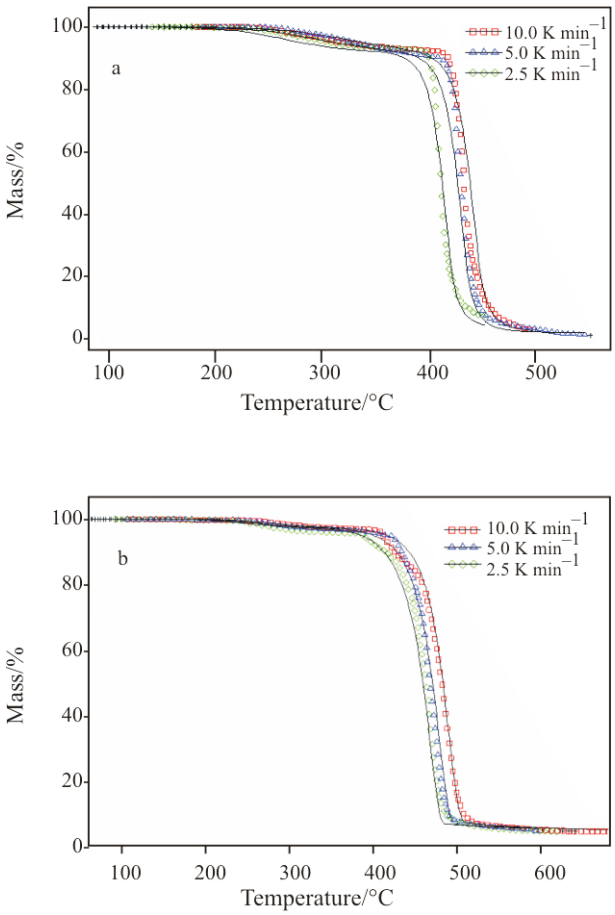

Fig. 6 Nonlinear kinetic modeling of a – PE and b – PE-MAPE-MMT thermal-oxidative degradation in air. Comparison between experimental TG data (dots) and the model results (firm lines) at several heating rates

Table 2 Results of the multiple-curve kinetic analyses for thermal-oxidative degradation of PE and PE-MAPE-MMT in accordance with the reaction model (5)

Material	Parameter	Value	Corr. Coeff.
PE	$\log A_1/s^{-1}$	3.7	0.9989
	E_1/kJ mol^{-1}	65.5	
	n_1	1.28	
	$\log A_2/s^{-1}$	15.5	
	E_2/kJ mol^{-1}	238.5	
	n_2	0.59	
	$\log A_3/s^{-1}$	16.9	
	E_3/ kJ/mol^{-1}	250.2	
	n_3	1.79	
PE-MAPE-MMT	$\log A_1/s^{-1}$	5.2	0.9992
	E_1/kJ mol^{-1}	87.5	
	n_3	1.34	
	$\log A_2/s^{-1}$	9.3	
	E_2/kJ mol^{-1}	166.2	
	n_2	0.78	
	$\log A_3/s^{-1}$	17.2	
	E_3/kJ mol^{-1}	279.6	
	n_3	0.89	

solid materials, the consumption of 1 kg of oxygen for their combustion is basically accompanied by evolution of 13.1 MJ of heat [25]. One of the tasks of this study was the correlation based evaluation of the heat release rate under the cone calorimetry test conditions and the rate of mass low under the conditions of isothermal pyrolysis in air. In the general form, the basic equation relating the mass loss rate to the heat release rate during combustion is as follows:

$$\dot{Q}_{tot}\,(\mathrm{k\ W\ m^{-2}}) = \chi \Delta H_{comb}\,\dot{m} \qquad (6)$$

where, χ is the combustion efficiency, ΔH_{comb} is the heat of complete combustion, and is the rate of mass loss per unit surface. If ΔH_{comb} is a constant value for PE and the PE-MAPE-MMT nanocomposite (i.e., the silicate additive does not inhibit gas-phase processes in the flame and has no effect on the heat of combustion), the heat release rate linearly depends on the mass loss rate. In this case, the coefficient χ for the linear equation characterizing the combustion efficiency or the completeness of combustion directly depends on the amount and structure of the carbonaceous residue.

It is clearly seen that under conditions of polymer ignition and initial surface combustion, the mass loss rate for PP-MAPE is noticeably lower than adequate values for the neat PE (Fig. 6). An improvement in flame resistance of PE-MAPE over the neat PE should happen as a result of the char formation providing a transient protective barrier. In the present study this phenomena was interpreted in terms of kinetic approach.

Flammability characteristics of PE and PE-MAPE-MMT nanocomposites

The flammability characteristics of pristine PE and PE-MAPE-MMT with 3 and 7 mass% Cloisite 20A nanocomposites were examined with a cone calorimeter at the incident heat flux of 35 kW m^{-2} for the samples having a standard surface area of 70×70 mm and identical masses of 12.0±0.2 g. Figures 8–10 depict the plots of the basic ignitability characteristics: heat release rate, mass loss rate, and specific heat of combustion, *vs.* time for PE, as well as for the PE-MAPE with 7 mass% of MMT and PE-MAPE with 3 mass% of MMT nanocomposites.

From Fig. 8, it is seen that the maximum heat release rate for pristine PE is 2005 kW m^{-2}, whereas that for the PE-MAPE-MMT (3 mass%) nanocomposite and the PE-MAPE-MMT (7 mass%) nanocomposite is 789 and 728 kW m^{-2}, respectively; thus, the peak heat release rate decreases by 40%. A similar trend is observed in Fig. 9, which illustrates the dependence of the mass low rate on the combustion time; Fig. 10 shows the time dependence for the specific heat of combustion, which is practically identical for all of the three samples. This resemblance con-

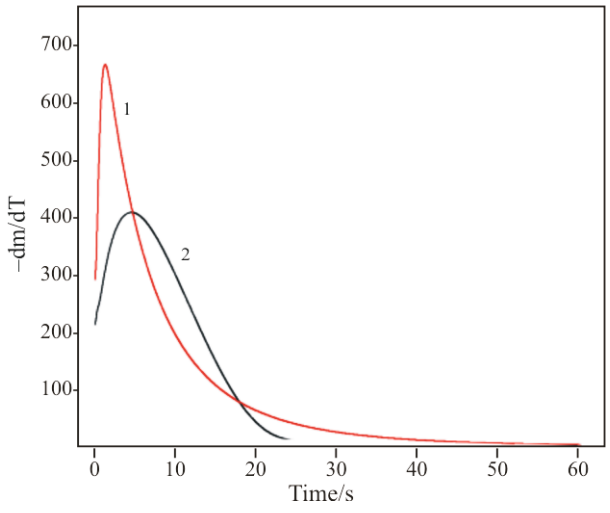

Fig. 7 Mass loss rates *vs.* time for 1 – PE and 2 – PE-MAPE-MMT under the isothermal heating condition at 600°C

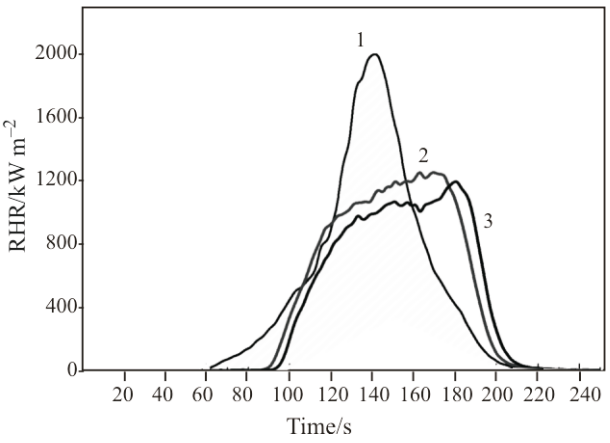

Fig. 8 Rate of heat release *vs.* time for 1 – PE, 2 – PE-MAPE-MMT (3 mass%) and 3 – PE-MAPE-MMT (7 mass%) obtained by cone calorimeter at the incident heat flux of 35 kW m^{-2}

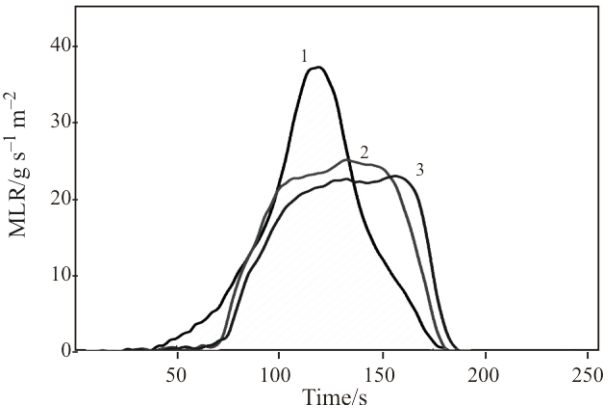

Fig. 9 Mass loss rate *vs.* time for 1 – PE, 2 – PE-MAPE-MMT (3 mass%) and 3 – PE-MAPE-MMT (7 mass%) obtained by cone calorimeter at the incident heat flux of 35 kW m^{-2}

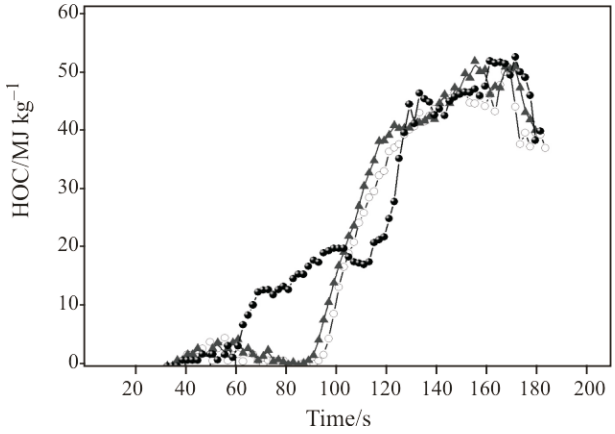

Fig. 10 Heat of combustion *vs.* time for ● – PE, ○ – PE-MAPE-MMT (3 mass%) and ▲ – PE-MAPE-MMT (7 mass%) obtained by cone calorimeter at the incident heat flux of 35 kW m^{-2}

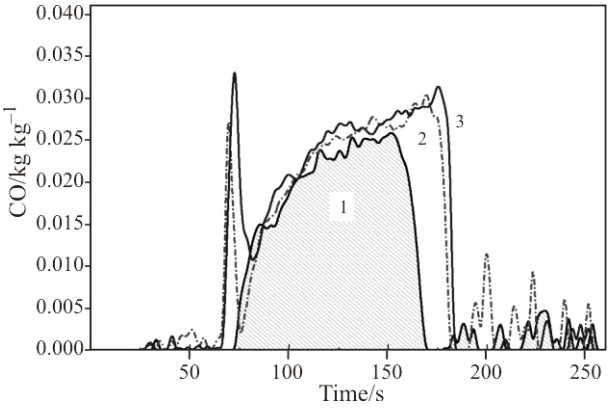

Fig. 11 CO yield *vs.* time for 1 – PE, 2 – PE-MAPE-MMT (3 mass%) and 3 – PE-MAPE-MMT (7 mass%) obtained by cone calorimeter at the incident heat flux of 35 kW m^{-2}

firms that the silicate agent does not inhibit the gas-phase combustion process and, thus, does not affect the heat of combustion of the samples; the effect of two-fold reduction in the maximum rate of heat release may be explained in terms of formation of a protective char layer on the burning polymer surface. The value characterizing the average amount of released carbon monoxide remains practically unchanged over the entire set of test samples; however, a small increase in the maximum CO yield for nanocomposite samples at the end of combustion time intervals indicates the crossover of active combustion to the oxygen-deficient smoldering phase (Fig. 11).

It is noteworthy that despite effective charring, the maximum level of smoke formation during the combustion of PE nanocomposites does not exceed the level of pristine PE, and its total yield is practically the same in all cases (Fig. 11).

The obtained results validate the conclusion that char formation plays a key role in the mechanism of flame retardation for nanocomposites. The sample surface coated with a composition of silicate particles and the heat-resistant organic ingredient of char is a very effective barrier on the way of flame propagation over the surface. The ideal structure of the protective layer containing silicate particles and organic char must be a densely crosslinked network structure and must possess a considerable mechanical strength sufficient for the protective layer to remain intact during the burning up of the polymer from the surface.

Conclusions

Dynamic TG experiments show substantial increase in thermal oxidative stability of the PE-MAPE-MMT nanocomposite as compared to pristine PE.

Collective action of chemical cross-linking and catalytic dehydration promoted by MMT presents a necessary and sufficient condition of solid phase carbonization reactions, which is observed in the process of thermal-oxidative degradation and combustion of PE-MAPE-MMT nanocomposites. Carbonized layer formation leads to appreciable increase of thermal stability of PE-MAPE-MMT nanocomposite, owing to a hindrance of the mass transfer in the nanocomposite. This fact explains an increase of thermal-oxidative stability in the PE-MAPE-MMT nanocomposite as well as its fire-proof properties.

Design data of the isothermal oxidative degradation at 600°C provided by the model kinetic analysis reveal substantial reduction of the mass loss rate of PE-MAPE-MMT nanocomposites as compared to pristine PE. These results are in close agreement with the experimental cone calorimeter tests performed at an incident heat flux of 35 kW m^{-2}.

References

1 D. J. Lacey and V. V. Dudler, Polym. Degrad. Stab., 51(1996) 1011.
2 M. Paabo and B. C. Levin, Fire Mater., 11 (1987) 55.
3 R. P. Lattimer, J. Anal. Appl. Pyrol., 31 (1995) 203.
4 T. Kuroki, T. Sawaguchi, S. Niikuni and T. Ikemura, Macromolecules, 15 (1982) 1460.
5 E. Kiran and J. K. Gillham, J. Anal. Appl. Pyrolysis, 20 (1976) 2045.
6 M. Blazso, J. Anal. Appl. Pyrolysis, 25 (1993) 25.
7 U. Hornung, A. Hornung and H. Bockhorn, Chem. Ing. Tech., 70 (1998) 145.
8 U. Hornung, A. Hornung and H. Bockhorn, Chem. Eng. Tech., 21 (1998) 332.
9 H. Bockhorn, A. Hornung and U. Hornung, J. Anal. Appl. Pyrolysis, 46 (1998) 1.
10 H. A. Bockhorn, A. Hornung, U. Hornung and D. Schawaller, J. Anal. Appl. Pyrolysis, 48 (1999) 93.

11 N. Grassie and S. Gerald, Polymer Degradation and Stabilization; Cambridge University Press, Cambridge–New York–Melbourne–Sydney 1988, p. 222.
12 L. Qiu, W. Chen and B. Qu, Polymer, 47 (2006) 922.
13 M. Zanetti, S. M. Lomakin and G. Camino, Macromol. Mater. Eng., 279 (2000) 1.
14 M. Alexandre and P. Dubois, Mater. Sci. Eng. R, 28 (2000) 1.
15 E. P. Giannelis, Adv. Mater., 8 (1996) 29.
16 J. W. Gilman, T. Kashiwagi, M. Nyden, J. T. Brown, C. L. Jackson, S. M. Lomakin, E. P. Gianellis and E. Manias, Chemistry and Technology of Polymer Additives, S. Al-Maliaka, A. Golovoy and C. A. Wilkie, Eds, Blackwell Scientific, London 1998, pp. 249–265.
17 M. Zanetti, P. Bracco and L. Costa, Polym. Degrad. Stab., 85 (2004) 657.
18 S. S. Ray and M. Okamoto, Prog. Polym. Sci., 28 (2003) 1539.
19 Y. Kojima, A. Usuki, M. Kawasumi, A. Okada, Y. Fukushima, T. Kurauchi and O. Kamigaito, J. Mater. Res., 8 (1993) 1185.
20 C. Breen, P. M. Last, S. Taylor and P. Komadel, Thermochim. Acta, 363 (2000) 93.
21 Z. Gao, I. Amasaki, T. Kaneko and M. Nakada, Polym. Degrad. Stab., 81 (2003) 125.
22 J. Jin Woo Park, S. Oh, H. Lee, H. Kim and K. Yoo, Polym. Degrad. Stab., 67 (2000) 535.
23 J. Opfermann, J. Therm. Anal. Cal., 60 (2000) 641.
24 D. Marquardt. J. Appl. Math., 11 (1963) 431.
25 V. Babrauskas, Fire Mater., 19 (1995) 243.
26 L. Lacoste and D. J. Carlsson, J. Polym. Sci. Part A, Polym. Chem., 30 (1992) 493.
27 F. Gugumus, Polym. Degrad. Stab., 76 (2002) 329.
28 F. Gugumus, Polym. Degrad. Stab., 77 (2002) 147.
29 S. W. Benson, Thermochemical Kinetics, Wiley, New York 1976, p. 114.
30 S. M. Lomakin, I. L. Dubnikova, S. M. Berezina and G. E. Zaikov, Polym. Int., 54 (2005) 999.
31 H. L. Friedman, J. Polym. Sci. C, 6 (1965) 175.

DOI: 10.1007/s10973-008-9355-x